A Layer-To-Layer Model and Feedback Control of Ink-Jet 3-D Printing

Lu Lu, *Member, IEEE*, Jian Zheng, and Sandipan Mishra, *Member, IEEE*

***Abstract*—Ink-jet 3-D printing is a promising additive manufacturing technology with the potential for impacting a wide variety of industries. In typical ink-jet 3-D printing, the part is built up by depositing droplets layer upon layer in an open-loop manner, while curing each layer after it is deposited. Droplet and edge dimensions are typically predicted through extensive experimentation and are assumed to remain constant throughout the printing process. However, there is no guarantee of the consistent droplet shape and dimensions or the smoothness of the finished parts due to the inherent uncertainty in the process. To address this issue, we propose a model-based feedback control law for ink-jet 3-D printing that uses a height sensor for measuring profile height after each layer for determining the appropriate layer patterns for subsequent layers. Toward this goal, a model describing the relationship between height profile change and droplet deposition in the layer building process is first proposed and experimentally identified. Based on this model, a closed-loop layer-to-layer control algorithm is then developed for the ink-jet printing process. The proposed algorithm uses a model predictive control algorithm to minimize the difference between the predicted height and the desired height and the predicted surface unevenness after a fixed number of layers. We also present an extension of the algorithm for two-material printing, which can enable printing of complex 3-D geometry (by using a support material for overhang). Experimental and simulation results show that the algorithm is able to achieve more consistent shapes between layers, reduced edge shrinking of the part, and a smoother top layer surface.**

***Index Terms*—Additive manufacturing (AM), mechatronics, motion control, predictive control, 3-D printing.**

I. Introduction

ADDITIVE manufacturing (AM) processes have recently seen a tremendous growth because of their potential to revolutionize manufacturing [1], [2]. Compared to the traditional ways of manufacturing based on material removal, additive manufacturing builds up parts layer by layer as shown in Fig. 1. A given (homogenous) part is first sliced into a sequence of layer patterns and each layer is built up based on these patterns. This process greatly reduces material waste and enables the manufacture of parts with geometries [3] that are nearly impossible or time consuming using traditional manufacturing methods.

Manuscript received April 10, 2014; accepted October 5, 2014. Recommended by Technical Editor H. Ding. This work was supported in part by NSF CAREER CMMI-1254313 and the Center for Automation Systems and Technologies, a NYSTAR funded center.

The authors are with the Center for Automation Technologies and Systems, Rensselaer Polytechnic Institute, Troy, NY 12180 USA (e-mail: lulu.lvlv@gmail.com; jzheng2188@gmail.com; mishrs2@rpi.edu).

Color versions of one or more of the figures in this paper are available online at http://ieeexplore.ieee.org.

Digital Object Identifier 10.1109/TMECH.2014.2366123

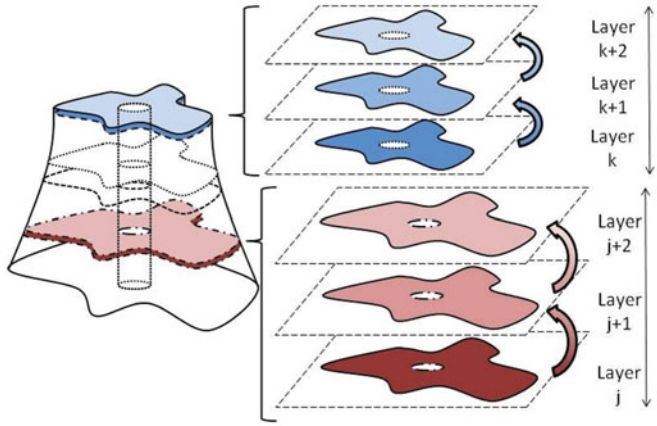

Fig. 1. Schematic of a typical layer-to-layer deposition process.

Typically, AM systems use polymers, plastic, ceramics, or metal in the form of liquid/waxy inks, filaments, or powder as the material to be deposited. The resolution of these commercial systems is usually limited by the size of the unit of deposition (droplet size, fiber diameter, or powder size) [4]. Specifically, ink-jet 3-D printing typically generates droplets with diameters between 50 and 500 μm, which vary depending on nozzle size, type of printing (thermal, piezo, or electrohydrodynamic), the material properties of the printed ink, among others [5]. The small size of this building unit (droplet) enables high resolution ink-jet 3-D printing.

The typical ink-jet 3-D printing system for photopolymeric ultraviolet (UV) curable inks consists of an XYZ stage that carries the substrate (or part), a nozzle (or nozzle array) that releases droplets, and an UV curing system. During the printing process, droplets are continuously ejected out of the nozzle and deposited onto the substrate layer by layer. After each layer is deposited, the part is exposed to an UV cure step so that the deposited liquid layer is solidified.

The typical ink-jet 3-D printing process is executed in an open-loop manner, i.e., the number of layers to be constructed and the droplet patterns to be deposited at each layer are determined in advance and do not change during the printing process based on any measurement of the true profile of the layer [4]. While this open-loop method is simple to implement, the final part often exhibits irregularities such as edge shrinking, unreliable dimensions, and surface unevenness. These undesirable phenomena are particularly obvious when the height of a part is large and the liquid material has a small contact angle with the surface, as evidenced by [6].

To address the issues of process uncertainty and irregular part geometry, simple models and closed-loop algorithms have been

developed, such as those in [7]–[9], [20]. In [7], wax droplets are deposited in a hexagonal tessellation and the shape of each droplet is modeled as a spherical cap. Then height maps of each spherical cap are obtained through the model introduced in [10]. By comparing the root mean square (RMS) error between the desired model and measurements, locations with errors higher than threshold are tagged as future deposition candidates. Thus, corrective action is taken only if the height has sufficiently large error. However, in these models, the interaction between adjacent wax droplets is ignored and the model does not consider the initial height of the working surface (i.e., each layer is assumed to be deposited on a flat surface). In [8], [20], the amount of edge shrinking is explicitly identified in advance and a compensation algorithm is designed to reduce the edge shrinking effect. This method is essentially feed-forward control in nature and does not account for in-process variability. Without incorporating the online profile height feedback, process uncertainties will degrade final part accuracy. In [9], a regression model is proposed to predict the thickness of the chemical vapor deposition process.

In contrast, feedback measurements have been used along with physics-based models in other additive manufacturing processes. For example, in [11], a laser metal deposition process is modeled through mass, momentum and energy balance to obtain the predicted profile of the printed part. Experimental results in the same work have shown the effectiveness of model-based feedback control in improving part resolution. In [12], a shape control algorithm is developed for overlaying one layer of a device to a previously printed layer in flash imprint lithography. Thus, there is clear indication that using model-based layer-to-layer control algorithms can improve performance of the ink-jet 3-D printing process.

Due to the nature of the deposited liquid material in ink-jet printing, the modeling methods used in [7] or [11] cannot be directly applied for ink-jet 3-D printing of liquids (such as photocurable polymers). In [13], a variable-line spacing printing scheme is proposed to maintain the droplet contact angle and achieve the desired pattern. By modifying line spacing, this algorithm is effective in building 2-D patterns. However, the proposed model is built assuming a flat working substrate, which cannot be directly applied in 3-D printing, where previously printed layers affect the geometry of subsequent layers.

In this paper, we present an extension of the results first demonstrated in [14]. In [14], a layer-to-layer height change model was proposed for ink-jet 3-D printing of liquid ink (photocurable polymer), based on which a closed-loop control algorithm was developed for a single-material printing process. In this paper, a comprehensive exposition of the problem including the quantitative analysis of the ability of the model to capture the edge shrinkage effect, a novel extension of the model and algorithm to two-material printing, detailed discussion of the computational issues, as well as the verification of the robustness of the algorithm through simulation have been added. This paper is organized as follows. First, a model describing the relationship between droplet deposition patterns and profile height change is proposed. In this model, it is assumed the *height change* at a point on the profile is affected by the droplet deposition at the point and its neighboring points. Then, a closed-loop layer-to-layer control algorithm is developed for the ink-jet printing process based on this model. Specifically, the proposed algorithm uses a model-based height prediction control algorithm to minimize the difference between the predicted height to the desired height and the predicted surface unevenness after a fixed number of layers. As an extension, the closed-loop algorithm for two-material printing is also proposed so that any arbitrarily complicated 3-D geometry can be printed with the help of support material. To demonstrate the performance of the proposed algorithm, experiments are conducted on an ink-jet printing system. The liquid ink used for printing is TangoPlus FullCure 930 (an UV curable ink). Experimental results show that the proposed algorithm achieves reduced edge shrinking, more consistent shapes between layers and smoother surface of the finishing layer compared to the open-loop algorithm.

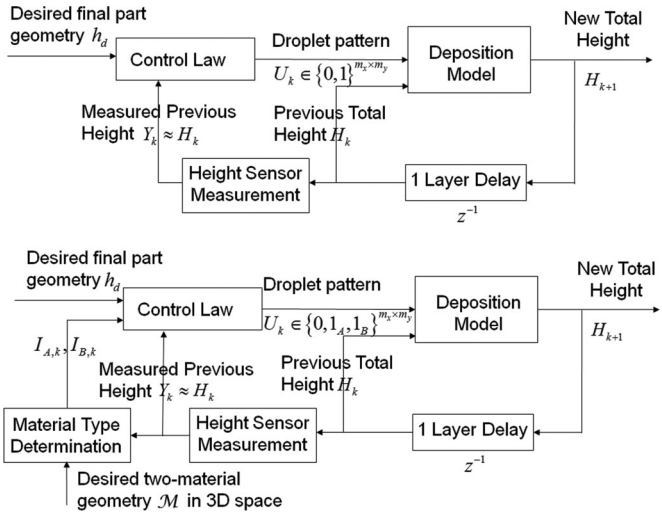

Fig. 2. Block diagram showing the closed-loop layer-to-layer printing process for (a) single-material printing and (b) two-material printing.

II. Problem Description

In this section, we present a general formulation of the model-based feedback control problem for layer-to-layer ink-jet 3-D printing. The overall block diagram of the system in this model-based layer-to-layer control framework is illustrated in Fig. 2 for single-material and two-material cases.

The control input to the ink-jet system (i.e., the plant) at the kth layer is the desired droplet pattern to be deposited, denoted by U_k. For single material printing, $U_k \in \{0,1\}^{m_x \times m_y}$ where $m_x \times m_y$ is the discretized grid size of the printing region. The integers 1 and 0 denote whether or not the droplet should be deposited onto the current location. For the two-material printing case, a point with $U_k = 1$ is further divided into two cases: deposition with material A or material B. Thus, $U_k \in \{0, 1_A, 1_B\}^{m_x \times m_y}$. The height profile of the existing surface is denoted by $H_k \in \{R^+\}^{m_x \times m_y}$. The deposition process (height change model), uses U_k and H_k to create the new layer. The overall height *after* the deposition is denoted by H_{k+1}, which is measured by the height/surface profile

Fig. 3. Coalescence process of two droplets (figure from [15]).

sensor. $h_d \in \{R^+\}^{m_x \times m_y}$ is the desired part geometry. Mathematically, the height change is modeled by $H_{k+1} = f_m(H_k, U_k)$, the height sensor measurement is given by $Y_k \approx H_k$. For single-material printing, the control law uses the final desired part geometry and the measured current height to generate the appropriate droplet patterns for subsequent layers, and the control law is given by $U_k = f_c(h_d, Y_k)$ or $U_k = f_c(h_d, H_k)$. For two-material printing, additional information is needed to determine which point should belong to which material at kth iteration. This information is characterized as two sets of points $I_{A,k}$ and $I_{B,k}$, which are obtained from the current layer height and the desired geometry of the part $\mathscr{M}$ in 3-D space, i.e., if the current grid point (i, j) with its corresponding height measured by the sensor (which gives a 3-D coordinate) belongs to $\mathscr{M}$, then this grid point is contained in $I_{A,k}$, otherwise it is contained in $I_{B,k}$. Thus, the control law for two-material printing is given by $U_k = f_c(h_d, I_{A,k}, I_{B,k}, Y_k)$ or $U_k = f_c(h_d, I_{A,k}, I_{B,k}, H_k)$.

To accurately control the geometric shape of the printed part, the following two problems need to be addressed:

1) the height change model f_m needs to be well identified to accurately capture the physical system;
2) the control law f_c must be designed to so that the final geometric shape of the object is as close to the desired shape as possible.

In the following two sections, we present a mathematical model f_m that characterizes the height change from layer-to-layer in Section III, and design a prediction-based control algorithm f_c based on the model in Section IV.

III. Height Change Model

Fig. 3 [15] shows how two liquid droplets coalesce into a spherical cap. From a purely physics-driven modeling approach, the height profile of formed part is complicated to model from a control-oriented perspective. Thus, an empirical model describing the 3-D droplets interaction during the layer-to-layer printing process will be developed.

Typically, the models proposed in additive manufacturing domain have focused on microlevel droplets coalescence [10], solidification of metal [11], plastic, and wax deposition [7]. However, these models cannot be directly applied to the ink-jet printing process because of the lack of consideration of the third (*Z*-axis) dimension or the fundamental difference in material properties (wax or metal, as opposed to liquid polymer). The height change model to be developed here should

1) be able to faithfully reflect how the height at certain point on the layer changes after a droplet is deposited with an acceptable degree of accuracy;
2) be simple enough for the model-based controller design. From a control design point of view, the second property is even more important than the first one. Generally speaking, as long as the model is simple enough for the controller design to use, a certain degree of modeling error may be tolerated since the closed-loop feedback can reduce the effect caused by the modeling error.

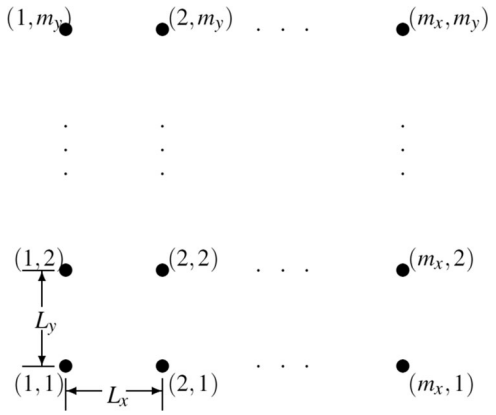

Fig. 4. Discretized printing region.

A. Single Layer Deposition on a Flat Surface

We now present our modeling approach for a single-layer deposition on a flat surface with one droplet material. Assume the entire printing region is a rectangle with a grid of droplets (note that this does not mean that the droplets are deposited everywhere on the grid resulting in a cuboidal part. This gridding is merely to characterize the overall spread of the part). When a layer is being printed, the droplets are deposited only at certain fixed points in the rectangular printing region. Letting m_x be the number of points in x-direction, and m_y be the number of points in y-direction, the entire printing region is discretized by an $m_x \times m_y$ grid, as shown in Fig. 4. It is critical to determine the line spacing (distance between center of droplets in the x and y directions) of the grid, namely L_x and L_y. Here, we choose these values based on the droplet diameter, i.e.

$$L_x = L_y = \gamma \cdot d \tag{1}$$

where d is the droplet diameter and γ is an optimal spacing factor. γ should be determined such that: 1) when all the points are printed onto a layer, the top layer(surface) is the smoothest and 2) any droplet does not overlap too much with its neighbors to prevent strong coalescing effect from happening. A small $\gamma < 0.5$ results in a smoother surface but has significant droplet coalescence, while a large $\gamma > 1$ results in a ribbed surface though there is no droplet coalescence. To determine γ for a given material and droplet diameter, some experiments need to be carried out, which will be detailed later in the experimental section.

After determining m_x, m_y and L_x, L_y, we can now present the height change model. First, we assume that for a particular point on the $m_x \times m_y$ grid, the droplets that affect its height change are categorized as center droplet, side droplets, and corner droplets. As plotted in Fig. 5(a), the blue, magenta, and green circles represent center droplet, side droplets, and corner

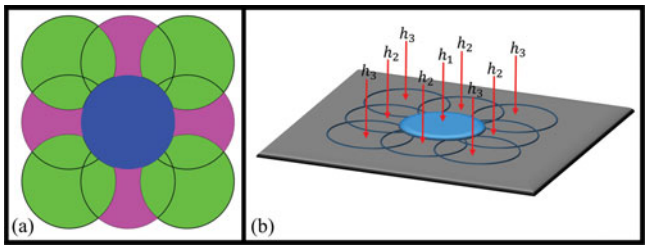

Fig. 5. (a) Droplet location categorization: blue-center droplet, magenta-side neighbors, green-corner neighbors. (b)Model illustration-height change parameters h_1, h_2, and h_3.

droplets, respectively. The height change is assumed to be the summation of all the height contributions of the aforementioned three types of droplets deposition. *It is key to note here that this is an approximation that only uses the two nearest-neighbors model, and the quality of the model can be improved by considering larger nearest-neighbor models*.

For this simplified model, we calculate each of the height contributions of the single droplet depositions on the nine points. To achieve this, let us assume only one droplet is deposited at a particular point and the height of that point equals the height of all its neighbors. The resulting height changes to the point itself, four side neighbors, and four corner neighbors are h_1, h_2, and h_3, respectively, as shown in Fig. 5(b). These parameters naturally vary for different inks and operating conditions, and will be identified in the experiment section.

Of course, for a single-layer deposition on a flat surface, this model is simple and yields the following equation describing the height change:

$$\begin{aligned}\Delta H_{i,j,k} = \; & h_1 U_{i,j,k} + h_2 (U_{i+1,j,k} \\ & + U_{i-1,j,k} + U_{i,j+1,k} \\ & + U_{i,j-1,k}) + h_3 (U_{i+1,j+1,k} \\ & + U_{i-1,j+1,k} \\ & + U_{i+1,j-1,k} + U_{i-1,j-1,k}) \\ \forall i = \; & 1, \cdots, m_x, \; j = 1, \cdots, m_y, \; k = 1, 2, \cdots\end{aligned} \tag{2}$$

where $\Delta H_{i,j,k}$ is the height increase at point (i, j) after the kth layer is printed, and $U_{i,j,k}$ is either 1 or 0 representing whether or not the droplet will be deposited at point (i, j) when $(k + 1)$th layer is being printed.

It should be noted that in the above height change model, the constants h_1, h_2, and h_3 are completely decoupled from the inputs $U_{i,j,k}$ at each point. h_1, h_2, and h_3 are inherent parameters of the system and do not depend on the desired geometry to be printed. When printing a complicated geometry such as an object with hollow part, the calculated inputs $U_{i,j,k}$ near the boundary may change from one to zero at each layer, but the constants h_1, h_2, and h_3 remain the same. In the two-material-printing case detailed later, h_1, h_2, and h_3 will change abruptly on the boundary. Thus, there will be some "discretization effect" on the geometric boundary. However, it is clear that such an effect only shows up at one or two pixels on the boundary, and will not affect the overall part accuracy dramatically.

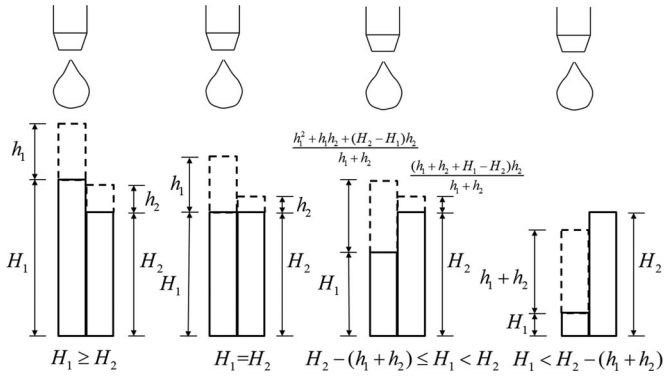

Fig. 6. Height change at center point and one of its side neighbors depending on the values of $H_1 - H_2$.

B. Layer-to-Layer Model Considering the Initial Height Profile

For predicting 3-D geometry of a part, the single-layer model proposed earlier is inadequate since the prior height profile is not taken into account. Thus, we now present a model that takes into account the initial height of the previous layer $H_{i,j,k}$ into consideration. With this modification, the actual height changes at the nine points for a single droplet deposition in the center will no longer be constants but functions of relative height between adjacent locations of the side neighbors, corner neighbors, and the center. Consider the side neighbors as a representative example. Fig. 6 shows how the height changes at the center location and one of its side neighbors vary depending on the relative heights between them on the previous layer. The "baseline" height increase at the center is h_1. The "additional" height increase h_2 will be distributed between the center and one of its side neighbors depending on the previous layer height at these two points. If the previous height at center is greater than or equal to that of the side neighbor, i.e., $H_1 \geq H_2$, the deposition of a new droplet on the center will cause the height at center to increase by h_1, and the height at the side neighbor to increase by h_2. However, if $H_1 < H_2$, the fluid will be constrained inside the center and the contribution to the height change at the side neighbor becomes smaller. As $H_1 - H_2$ decreases, the height change at the side neighbor will continue to decrease until $H_1 = H_2 - (h_1 + h_2)$. From then on, the height at the side neighbor does not increase any more since it is much higher than the center point (fluid will all be constrained in the center). This "neighboring points" model ensures that the height change summation for the center point and side neighbor is always equal to $h_1 + h_2$ no matter what value $H_1 - H_2$ is. This is consistent with mass conservation since the droplet volume is fixed and does not depend on the profile height. Similar analysis can be performed on the other side neighbors and the corner neighbors. Finally, the total height change at the center is equal to h_1 plus an additional term depending on how much fluid "flows back" to the center due to the unevenness of the previous layer.

The height change from kth layer to $(k+1)$th layer is given by

$$\begin{aligned} H_{i,j,k+1} = \; & H_{i,j,k} + C_1 + C_2 + C_3 \\ \forall i = \; & 1, \ldots, m_x, \; j = 1, \ldots, m_y, \; k = 1, 2, \ldots . \end{aligned} \tag{3}$$

In the aforementioned model, the height change at point (i, j) is the linear contribution of the following three height change functions:
C_1— the height change resulted from the droplet depositing at point (i, j);
C_2— the height change resulted from the droplet depositing at four side neighbors of point (i, j), i.e., $(i+1, j)$, $(i-1, j)$, $(i, j+1)$, and $(i, j-1)$;
C_3— the height change resulted from the droplet depositing at four corner neighbors of point (i, j), i.e., $(i+1, j+1)$, $(i+1, j-1)$, $(i-1, j+1)$ and $(i-1, j-1)$.

Based on the aforementioned analysis, the terms C_1, C_2, and C_3 are formulated as follows:

$$\begin{aligned} C_1 = \; & U_{i,j,k} \cdot \{h_1 + 4h_2 + 4h_3 - h_2[\text{sat}_{h_1+h_2}(H_{i,j,k} \\ & - H_{i+1,j,k}) + \text{sat}_{h_1+h_2}(H_{i,j,k} - H_{i-1,j,k}) \\ & + \text{sat}_{h_1+h_2}(H_{i,j,k} - H_{i,j+1,k}) \\ & + \text{sat}_{h_1+h_2}(H_{i,j,k} - H_{i,j-1,k})] \\ & - h_3[\text{sat}_{h_1+h_3}(H_{i,j,k} - H_{i+1,j+1,k}) \\ & + \text{sat}_{h_1+h_3}(H_{i,j,k} - H_{i+1,j-1,k}) + \\ & \text{sat}_{h_1+h_3}(H_{i,j,k} - H_{i-1,j+1,k}) \\ & + \text{sat}_{h_1+h_3}(H_{i,j,k} - H_{i-1,j-1,k})], \} \\ C_2 = \; & h_2[U_{i+1,j,k} \cdot \text{sat}_{h_1+h_2}(H_{i+1,j,k} - H_{i,j,k}) \\ & + U_{i-1,j,k} \cdot \text{sat}_{h_1+h_2}(H_{i-1,j,k} - H_{i,j,k}) \\ & + U_{i,j+1,k} \cdot \text{sat}_{h_1+h_2}(H_{i,j+1,k} - H_{i,j,k}) \\ & + U_{i,j-1,k} \cdot \text{sat}_{h_1+h_2}(H_{i,j-1,k} - H_{i,j,k})], \\ C_3 = \; & h_3[U_{i+1,j+1,k} \cdot \text{sat}_{h_1+h_3} \\ & (H_{i+1,j+1,k} - H_{i,j,k}) \\ & + U_{i+1,j-1,k} \cdot \text{sat}_{h_1+h_3} \\ & (H_{i+1,j-1,k} - H_{i,j,k}) \\ & + U_{i-1,j+1,k} \cdot \text{sat}_{h_1+h_3} \\ & (H_{i-1,j+1,k} - H_{i,j,k}) \\ & + U_{i-1,j-1,k} \cdot \text{sat}_{h_1+h_3} \\ & (H_{i-1,j-1,k} - H_{i,j,k})] \end{aligned} \tag{4}$$

where h_1, h_2, and h_3 are the height change constants for "center," "side," and "corner" points, respectively. The saturation function $\text{sat}_*(\bullet)$ characterizes how the neighboring point's height changes in terms of the current height difference between the two points, and is defined by

$$\text{sat}_a(b) = \begin{cases} 1, & \text{if } b \geq 0 \\ 1 + \dfrac{b}{a}, & \text{if } -a \leq b < 0 \\ 0, & \text{else.} \end{cases} \tag{5}$$

It is noted here that the term C_1 depends not only on h_1, but also on h_2 and h_3 since the side and corner neighbors can affect the height at the center through the parameters h_2 and h_3. However, the terms C_2 and C_3 depend only on h_2 and h_3 since h_1 only represents the "baseline" height change at center and does not characterize the interaction effect between neighbors.

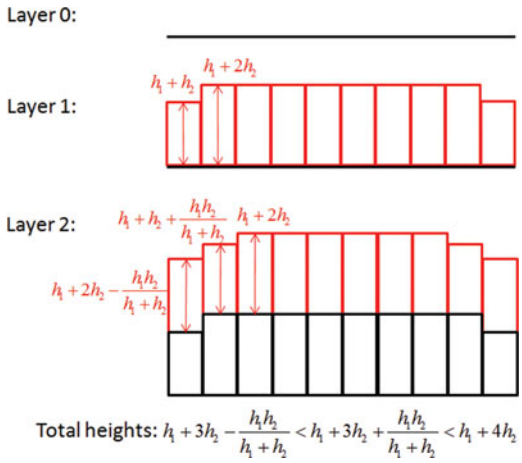

Fig. 7. Illustration of the edge shrinkage effect after two-layers of printing.

C. Justification of the Model

One of the key advantages of the proposed model over a simple "additive" model is that it is able to capture the edge shrinkage effect observed in printing after several layers are printed (unlike the simple additive model). This shrinkage effect is typically caused by the flow of ink liquid from the center of deposition to its neighboring locations that are not significantly higher as well as surface tension, which is captured (in an empirical manner) by the proposed model through the parameters h_1, h_2, and h_3.

We now explain qualitatively how the shrinkage can be captured by the proposed model. As illustrated in Fig. 7, suppose there are N points in an 1-D array (i.e., a line), initially all at the same height. After one layer of deposition, the height of all the points increases by $h_1 + 2h_2$ because of the flow of liquid to the neighbors, except for the two points on the edges whose height only increases by $h_1 + h_2$ due to the lack of droplet deposition on their outer side. Thus, after the first layer of deposition, the edge shrinkage effect is already observed on the two edge points. In the second layer of deposition, since the height at edge points are lower than the height at "near edge points," part of liquid (represented by h_2) will flow back from the "near edge points" to the edge points. According to the formula, the height at edge points increases by $h_1 + 2h_2 - \frac{h_1 h_2}{h_1+h_2}$, and the height at "near edge points" increases by $h_1 + h_2 + \frac{h_1 h_2}{h_1+h_2}$, and the height at all the other points still increases by $h_1 + 2h_2$. The

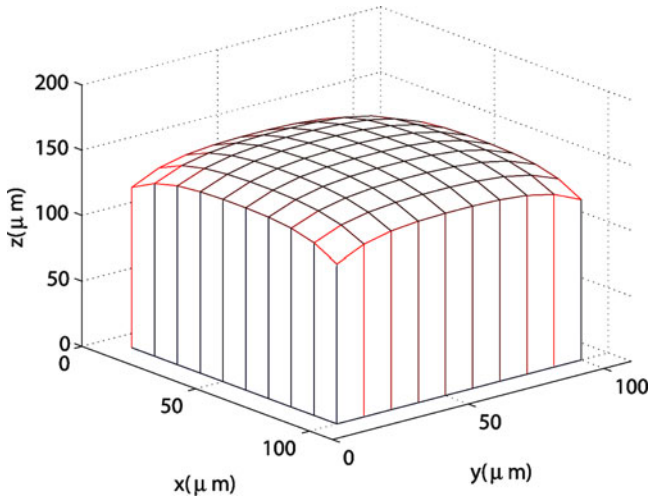

Fig. 8. Six-layer open-loop printing simulation using the proposed model. Note the edge shrinkage effect, as captured by the proposed model.

total heights are $2h_1 + 3h_2 - \frac{h_1 h_2}{h_1+h_2}$, $2h_1 + 3h_2 + \frac{h_1 h_2}{h_1+h_2}$, and $2h_1 + 4h_2$ at edge points, "near edge points" and all the other points, respectively. Thus, the overall height profile after two layers of deposition shows a gradual shrinkage at two points near the edges. It can be easily derived that after M layers of deposition, the gradual edge shrinkage can be seen at M points near the edges. Fig. 8 shows the simulation result of the total height after ten-layer open-loop printing of a cylindrical part ($U_{i,j,k} = 1\ \forall i, j, k$) with the proposed model used to predict the part geometry. From the figure, we see that the model is able to capture edge shrinkage effect. On the other hand, the simple additive model is unable to capture the edge shrinkage effect.

D. Extension of the Proposed Model to Two-Material Printing

In the previous sections, the height change model is proposed for printing on a rectangle area using one droplet material. In typical 3-D printing applications, the printed 3-D object may be of complicated shape with convex or nonconvex (concave) geometry. In the traditional rapid prototyping technology, such a complicated geometry is printed with two different materials—object material and sacrificial material. The sacrificial material is used to support the object that may have many concave parts during the manufacturing process, and is washed away when the process is done. Specifically, the complicated geometry of the object is first cut into thin layers with rectangular shape inside the computer. On each rectangular layer, the solid part with object is marked as "object material" and the hollow part is marked as "sacrificial material." When each layer is constructed during the prototyping process, the points with "object material" marker is printed with object material and the points with "sacrificial material" marker is printed with sacrificial material. The process goes on until all the layers are generated [16].

Ink-jet 3-D printing with multiple materials is challenging for several reasons. One of the reasons has to do with the complexity and uncertainty of the layer-to-layer height change model of the such an ink-jet printing process. The traditional rapid prototyping technique uses the metal powder or plastic to form layers. The layer height is easy to control in an open-loop manner and is assumed to be a known constant across the working region. No real-time closed-loop control is needed beyond the high-level supervisory monitoring [17]. However, due to the high liquidity of the material, the height change model in an ink-jet printing process is much more complicated and involves more uncertainties across the printing region. For two-material printing, it is necessary to construct an accurate height change model of the object and use real-time feedback and control to deposit the object material and sacrificial material into their correct locations. In the following section, a layer-to-layer height change model for two-material printing is presented, which lays down the foundation for closed-loop control.

As before, we assume that the printing region is rectangular and is discretized by an $m_x \times m_y$ grid. For a single-layer deposition on a flat surface, a droplet of object material (material A) deposited at certain point causes height changes of h_1, h_2, and h_3 on the point itself, its side neighbors and corner neighbors. A droplet of sacrificial material (material B) deposited at certain point causes height changes of g_1, g_2, and g_3 on the point itself, its side neighbors and corner neighbors. The height change at point i, j is, thus, given by

$$\begin{aligned} H_{i,j,k+1} = \ & H_{i,j,k} + h_{1|i,j,k}U_{i,j,k} \\ & + h_{2|i+1,j,k}U_{i+1,j,k} \\ & + h_{2|i-1,j,k}U_{i-1,j,k} \\ & + h_{2|i,j+1,k}U_{i,j+1,k} \\ & + h_{2|i,j-1,k}U_{i,j-1,k} \\ & + h_{3|i+1,j+1,k}U_{i+1,j+1,k} \\ & + h_{3|i-1,j+1,k}U_{i-1,j+1,k} \\ & + h_{3|i+1,j-1,k}U_{i+1,j-1,k} \\ & + h_{3|i-1,j-1,k}U_{i-1,j-1,k} \\ \forall i = \ & 1, \cdots, m_x,\ j = 1, \cdots, m_y,\ k = 1, 2, \cdots \end{aligned} \quad (6)$$

where $h_{1|i,j,k} = h_1$, $h_{2|i,j,k} = h_2$, and $h_{3|i,j,k} = h_3$ when $(i, j) \in I_{A,k}$, i.e., the point (i, j) on kth layer is printed with material A. $h_{1|i,j,k} = g_1$, $h_{2|i,j,k} = g_2$ and $h_{3|i,j,k} = g_3$ when $(i, j) \in I_{B,k}$, i.e., the point (i, j) on kth layer is printed with material B.

When the initial height $H_{i,j,k}$ is different across the printing region, the C_1, C_2, and C_3 terms in (3) are given as follows:

$$\begin{aligned} C_1 = \ & U_{i,j,k} \cdot \Big\{ h_{1|i,j,k} + 4h_{2|i,j,k} + 4h_{3|i,j,k} \\ & - h_{2|i,j,k}[\text{sat}_{h_{1|i,j,k}+h_{2|i,j,k}}(H_{i,j,k} - H_{i+1,j,k}) \\ & + \text{sat}_{h_{1|i,j,k}+h_{2|i,j,k}}(H_{i,j,k} - H_{i-1,j,k}) \\ & + \text{sat}_{h_{1|i,j,k}+h_{2|i,j,k}}(H_{i,j,k} - H_{i,j+1,k}) \\ & + \text{sat}_{h_{1|i,j,k}+h_{2|i,j,k}}(H_{i,j,k} - H_{i,j-1,k})] \\ & - h_{3|i,j,k}[sat_{h_1+h_{3|i,j,k}}(H_{i,j,k} - H_{i+1,j+1,k}) \\ & + \text{sat}_{h_{1|i,j,k}+h_{3|i,j,k}}(H_{i,j,k} - H_{i+1,j-1,k}) \\ & + \text{sat}_{h_{1|i,j,k}+h_{3|i,j,k}}(H_{i,j,k} - H_{i-1,j+1,k}) \end{aligned}$$

$$
\begin{aligned}
&+ \text{sat}_{h_{1|i,j,k}+h_{3|i,j,k}}(H_{1,j,k} - H_{1-1,j-1,k})]\Big\}\\
C_2 = \;& h_{2|i+1,j,k}U_{i+1,j,k} \cdot \text{sat}_{h_{1|i+1,j,k}} + h_{2|i+1,j,k}\\
&(H_{i+1,j,k} - H_{i,j,k}) + h_{2|i-1,j,k}U_{i-1,j,k}\\
&\cdot\text{sat}_{h_{1|i-1,j,k}+h_{2|i-1,j,k}}(H_{i-1,j,k} - H_{i,j,k})\\
&+ h_{2|i,j+1,k}U_{i,j+1,k} \cdot \text{sat}_{h_{1|i,j+1,k}} + h_{2|i,j+1,k}\\
&- (H_{i,j+1,k}H_{i,j,k}) + h_{2|i,j-1,k}U_{i,j-1,k}\\
&\cdot\text{sat}_{h_{1|i,j-1,k}+h_{2|i,j-1,k}}(H_{i,j-1,k} - H_{i,j,k}),\\
C_3 = \;& h_{3|i+1,j+1,k}U_{i+1,j+1,k} \cdot \text{sat}_{h_{1|i+1,j+1,k}+h_{3|i+1,j+1,k}}\\
&(H_{i+1,j+1,k} - H_{i,j,k}) + h_{3|i+1,j-1,k}U_{i+1,j-1,k}\\
&\cdot\text{sat}_{h_{1|i+1,j-1,k}+h_{3|i+1,j-1,k}}(H_{i+1,j-1,k} - H_{i,j,k})\\
&+ h_{3|i-1,j+1,k}U_{i-1,j+1,k} \cdot \text{sat}_{h_{1|i-1,j+1,k}+h_{3|i-1,j+1,k}}\\
&(H_{i-1,j+1,k} - H_{i,j,k}) + h_{3|i-1,j-1,k}U_{i-1,j-1,k}\\
&\cdot\text{sat}_{h_{1|i-1,j-1,k}+h_{3|i-1,j-1,k}}(H_{i-1,j-1,k} - H_{i,j,k}). \qquad (7)
\end{aligned}
$$

IV. Control Algorithm

In this section, we present a layer-to-layer control algorithm based on the model proposed in the previous section. We first develop a control algorithm for the single material case, and then, propose an extension of this algorithm to the two-material (multimaterial) generalization. Finally, we discuss the computational issue regarding the proposed prediction-based control algorithm.

A. Single-Material Control Algorithm

We assume that that the object to be printed has uniform shape at each layer (in other words, the object can be constructed by pure extrusion). The extension to nonextended shape is presented in Section IV-B. Suppose the desired profile height is h_d, the control inputs are $U_{i,j,k}\ \forall 1 \le i \le m_x, 1 \le j \le m_y,\ k \in \mathbb{N}$ and the height at all the points on all the layers (i.e., $H_{i,j,k}\ \forall 1 \le i \le m_x, 1 \le j \le m_y,\ k \in \mathbb{N}$) can be measured. The objective is to design a feedback control law such that the heights of all the points on the final layer (finishing layer) are as close to h_d as possible. It should be noted that this objective automatically incorporates three requirements: consistent shapes between layers, minimum edge shrinkage, and minimum surface unevenness of the top layer. Clearly, if the objective is perfectly met, the shapes at each layer will be exactly the same, the edge shrinkage does not occur, and the surface of the top layer is perfectly smooth.

Specifically, before printing the kth layer, the control command $U_{i,j,k}$ is calculated by solving the minimization algorithm,

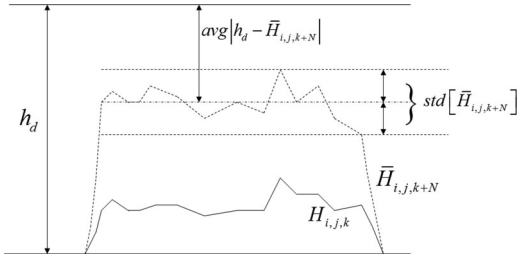

Fig. 9. Illustration of the proposed prediction control algorithm.

(8), shown at the bottom of the page. As shown in Fig. 9, avg(•) and std(•) are the mean and standard deviation functions, respectively. $\bar{H}$ is the predicted height, $\bar{U}$ is the set of future control inputs to be optimized. N is the number of layers in prediction horizon. The objective function is a combination of two terms: the average of the differences between the desired height and the height of each point after N layers, and the standard deviation of the profile height after N layers. α is the weighting constant for the two terms. It should be noted that the predicted height $\bar{H}$ is derived from the current measured layer height H, which is used as the initial condition, as seen in the last equation of (8). Thus, the objective function explicitly depends on the height measurement.

At the initial stages of printing when the profile height is much lower than the desired height h_d, the first term tries to add as many droplets deposited onto the layer as possible in order to quickly drive the height to the desired value, while the second term tries to maintain consistent height among all the points on the layer. This is similar to letting a row of people running forward as fast as possible, and at the same time attempting to keep the row formation. As the profile height gets close to the desired one, the first term (since it is an absolute value) prevents the height overshoot from happening, and the second term tries to minimize the surface unevenness of the top layer.

With proper choice of α, the algorithm is able to achieve consistent shape between layers, minimum edge shrinkage as well as minimum surface unevenness compared to the open-loop control. By changing α from layer-to-layer, we can also further tune the performance. The effectiveness of the proposed algorithm will be shown later in the next section.

B. Extension to Two-Material Printing

The proposed control algorithm can be easily extended to two-material printing, which can be used for nonextruded shape. The optimization algorithm to be solved is still the same as (8). The only difference is that for two-material case, the set $I_{A,k}$ and $I_{B,k}$ need to be identified, i.e, where to deposit material

$$
\min_{\substack{\bar{U}_{i,j,k}\ \forall 1\le i\le m_x \\ 1\le j\le m_y,\, k\le \bar{k}<k+N}} \left\{\alpha \cdot \operatorname*{avg}_{\substack{1\le i\le m_x \\ 1\le j\le m_y}} |h_d - \bar{H}(i,j,k+N)| + (1-\alpha)\cdot \operatorname*{std}_{\substack{1\le i\le m_x \\ 1\le j\le m_y}} [\bar{H}(i,j,k+N)]\right\}
$$

$$
\text{subject to} \qquad (8)
$$

$$
\bar{H}(i,j,\bar{k}+1) = \bar{H}(i,j,\bar{k}) + \bar{C}_1 + \bar{C}_2 + \bar{C}_3 \ \ \forall k \le \bar{k} < k+N,\quad \bar{H}(i,j,k) = H(i,j,k).
$$

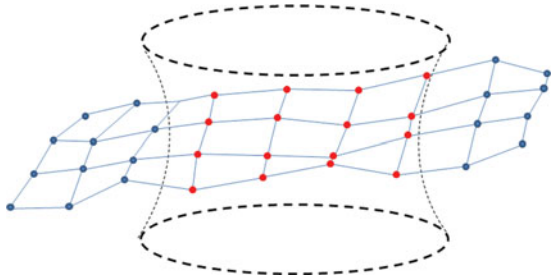

Fig. 10. Illustration of how to determine $I_{A,k}$ and $I_{B,k}$. The desired geometry is represented by dashed black line. $I_{A,k}$ is the collection of all the red points on kth layer (inside the desired geometry). $I_{B,k}$ is the collection of all the blue points on kth layer (outside the desired geometry).

A or material B on the kth layer needs to be determined. Here, we use a simple decision criterion to identify $I_{A,k}$ and $I_{B,k}$ as shown in Fig. 10. Suppose the geometry of the system is given by a set $\mathscr{M} \subset \mathscr{C}$, where $\mathscr{C} \triangleq \{(x,y,z)|0 \le x \le L_x m_x,\ 0 \le y \le L_y m_y,\ 0 \le z \le h_d\}$ is a 3-D cuboid. A point (i,j,k) in the grid coordinate belongs to $I_{A,k}$ iff the point $(iL_x, jL_y, H_{i,j,k}) \in \mathscr{M}$ in 3-D Euclidean space, and belongs to $I_{B,k}$ iff the point $(iL_x, jL_y, H_{i,j,k}) \in \bar{\mathscr{M}}$ in 3-D Euclidean space.

At each iteration, this decision procedure is carried out after the measurement of the layer height is obtained. Then, the sets $I_{A,k}$ and $I_{B,k}$, which are then used in solving Problem (8) for deposition of different materials onto different locations.

In real applications, the set $\mathscr{M}$ may be determined analytically or numerically. For geometry with analytical expression, we define $\mathscr{M}$ analytically. For example, a vertical pipe can be represented by $\mathscr{M} \triangleq \{(x,y,z)|r_1^2 \le (x-x_c)^2 + (y-y_c)^2 \le r_2^2,\ 0 \le z \le h_d\}$, where r_1 and r_2 are the inner and outer radius, respectively, and (x_c, y_c) is the projection of center axis on to the $x-y$ plane. For more complicated geometry with no analytical formula available, numerical discretization may be carried out to represent $\mathscr{M}$ as the union of multiple small units (such as cuboid).

C. Computational Issues

Problem (8) is a large-scale constrained integer programming problem with the optimization variables being binary numbers. The function needs to be optimized for all $U_{i,j,\bar{k}}$ with $1 \le i \le m_x, 1 \le j \le m_y$, and $k \le \bar{k} < k+N$. Although each of the variables only takes the value of either 0 or 1, the total number of combinations is $2^{m_x \times m_y \times N}$, which increases dramatically with the size of the grid and number of prediction layers. This is well known as the "curse of dimensionality" for numerical optimization [18]. For this kind of large-scale nonlinear programming problem, there does not exist any algorithm that can theoretically guarantee the convergence to global optimum. It is possible to reduce N, e.g., the prediction can be made as small as 1. But the grid size parameters m_x and m_y can not be reduced. For large m_x and m_y, it is generally not possible to obtain the global minima in a deterministic manner due to these computational issues. Two main classes of solutions exist as to restricting the dimension of optimization space to shorten the computational time [19]. The first class of solutions utilizes some stochastic operations in each iteration, e.g., genetic algorithm and simulated annealing. The second one employs certain greedy-type search algorithms to find the next optimal state around the neighborhood of the current state in each iteration.

Considering the fact that the algorithm complexity is high for large m_x and m_y, we develop an efficient algorithm combining the advantages of both deterministic and stochastic method, which will be called "stochastic greedy-type search algorithm." Specifically, we start with an initial guess $\bar{U}_{(0)i,j,\bar{k}}$ (whose elements could be all zero or all one). Then, we randomly pick up a small subset of M points within $\{(i,j,k)|1 \le i \le m_x, 1 \le j \le m_y, 1 \le k \le N\}$. For each point, we "flip" the corresponding $\bar{U}$ (change it from 0 to 1 or from 1 to 0) to see if it gives smaller objective function. If it does, then mark it as "Y." After the inspection of all the points inside the subset is done, we flip all the point marked as "Y." Note that this procedure takes only $M \times N$ steps (which does not depend on the grid size m_x and m_y) since each time only one variable (element) is allowed to be flipped inside the subset. The process keeps going on until no flip is found to achieve smaller objective function value even if $M = 1$ and the flipping of all the single points are tested. In practice, we can set an upper bound for the highest number of iterations allowed.

Although this algorithm does not theoretically guarantee convergence at global minima, we claim that it clearly performs better than the open-loop algorithm if we use the open-loop input as initial guess for the solution since the cost function monotonically decreases at each step. This definitely makes the closed-loop algorithm a better choice than the simple open-loop algorithm in experiments provided the height measurement is available. Thus, there is value added by the algorithm since it is able to locally obtain a better print pattern than open-loop control.

In order to provide the reader with an illustration of how close the solution given by our algorithm may be to the global solution, we perform a simple simulation test. We consider a 20×20 grid with certain random initial height $H_{\rm ini}$, and set the input matrix $U_{\rm rad}$ to be consisting of random 0 and 1 numbers. This input matrix is fed to $H_{\rm ini}$ and generate a new layer height $H_{\rm new}$ after a single-layer deposition. Now, we set $\alpha = 1$ in the algorithm so that only the first part of the objective function is considered, and set the desired height to be $H_{\rm new}$ and initial height as $H_{\rm ini}$. In this case, it is clear that the exact solution is $U_{\rm rad}$ since the objective function goes to zero. Then, we start at a different initial guess with $U_{i,j,k} = 1$ at all point (open-loop algorithm), and use the same algorithm to iterate and search for optimal solution. We found that our algorithm is able to reach the exact solution for all the 50 different (random) combinations of $H_{\rm ini}$ and $U_{\rm rad}$ we have tried. Although this is merely an anecdotal it nevertheless shows how close the solution given by our algorithm is to the exact solution in general. Furthermore, it does give satisfactory results in our physical experiments, which will be shown later in the next section.

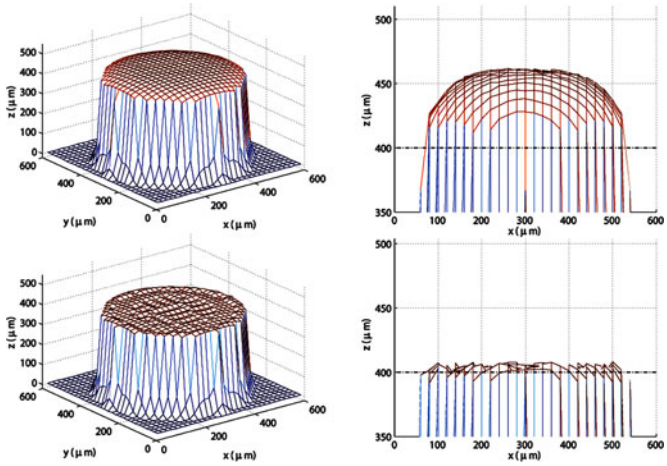

Fig. 11. Simulation of open-loop (top) and closed-loop (bottom) printed cylinder for 20% variation on h_1, h_2, and h_3. The desired height of the cylinder is $400\,\mu\mathrm{m}$. The open-loop one shows dome-shaped top surface and the closed-loop one shows flat top surface. The mean errors for open-loop and closed-loop surfaces are 44.1 and $0.7\,\mu\mathrm{m}$, respectively. The standard deviations are 15.0 and $4.1\,\mu\mathrm{m}$, respectively.

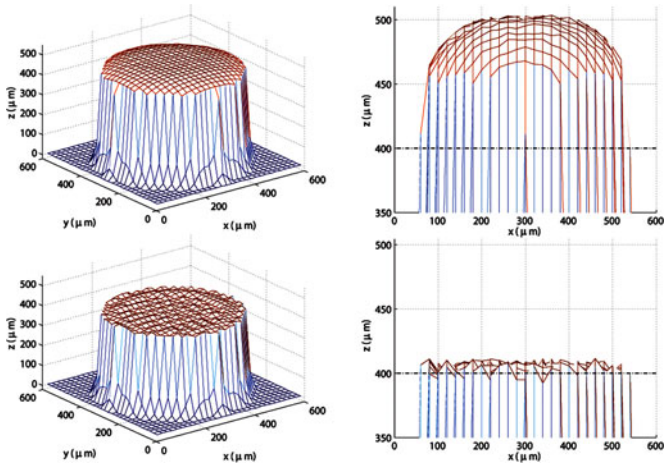

Fig. 12. Simulation of open-loop (top) and closed-loop (bottom) printed cylinder for 40% variation on h_1, h_2, and h_3. The desired height of the cylinder is $400\,\mu\mathrm{m}$. The open-loop one shows dome-shaped top surface and the closed-loop one shows flat top surface. The mean errors for open-loop and closed-loop surfaces are 84.7 and $1.9\,\mu\mathrm{m}$, respectively. The standard deviations are 16.6 and $4.5\,\mu\mathrm{m}$, respectively.

V. Results

A. Simulation

We first run the proposed algorithm in simulation. Figs. 11 and 12 show the aerial and side views of two cylinders printed with open-loop and closed-control printing algorithm for $[0\ 20\%]$ and $[0\ 40\%]$ variations on h_1, h_2, and h_3, respectively, as is typical for these printing applications. The desired height of the cylinder is $400\,\mu\mathrm{m}$. From the figures, it is seen that the top section of the open-loop printed cylinder looks like a dome structure. And as the percentage of uncertainties increases, the deviation of the actual height from the desired height also increases. On the other hand, the cylinder printed with closed-loop control has a much

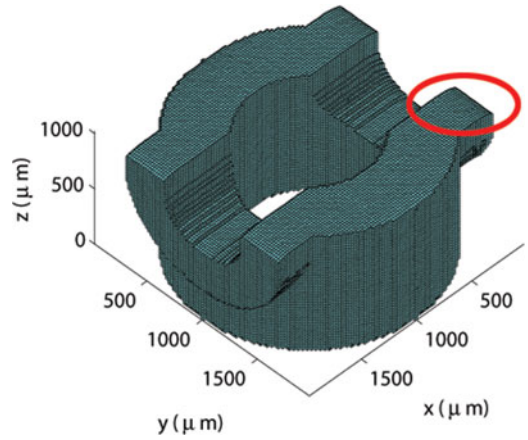

Fig. 13. Two-material open-loop printing of the junction section of two pipes.

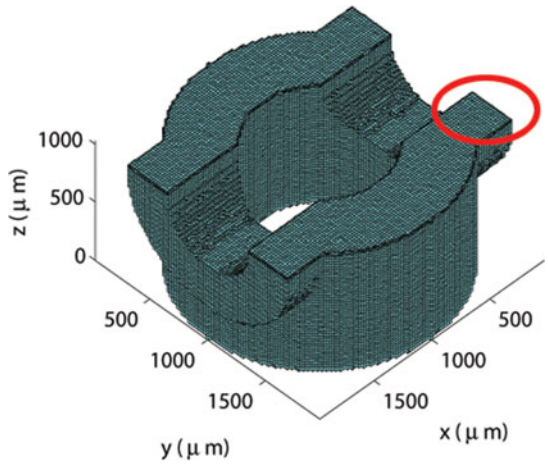

Fig. 14. Two-material closed-loop printing of the junction section of two pipes.

flatter top surface whose height is close to the desired height even when the uncertainty reached 40%. The quantitative results for open-loop and closed-loop printing methods (the mean error and standard deviation) are shown in the captions of the figures. It is noted that the "dome" structure is caused by the flowing of the liquid from the center point to its neighbors as explained in the modeling section. The simulation results show the effectiveness of the proposed algorithm in better achieving the desired height at all the points across the top layer, and the robustness of the algorithm with respect to the uncertainty of droplet size.

Next, the proposed two-material printing algorithm is implemented to print a more complicated structure—the junction section of two pipes. The grid size is 100×100. The printed result (the object material part) for the open-loop printing method (assuming a fixed layer height) and the closed-loop printing method are shown in Figs. 13 and 14. It can be seen that the open-loop printed object has visible deformation near the edge, as circled in red. In comparison, with the proposed algorithm, the printed object can accurately represent the desired geometry with no visible deformation. The top surface is almost flat. Fig. 15 shows the entire printing block including both sacrificial

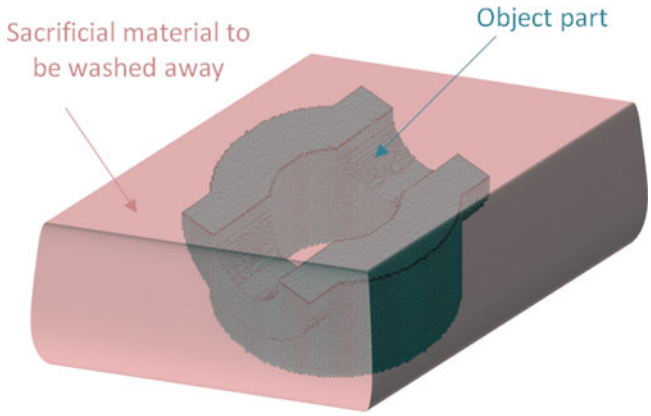

Fig. 15. Schematics showing that sacrificial material should be washed away/removed and the object part is then obtained.

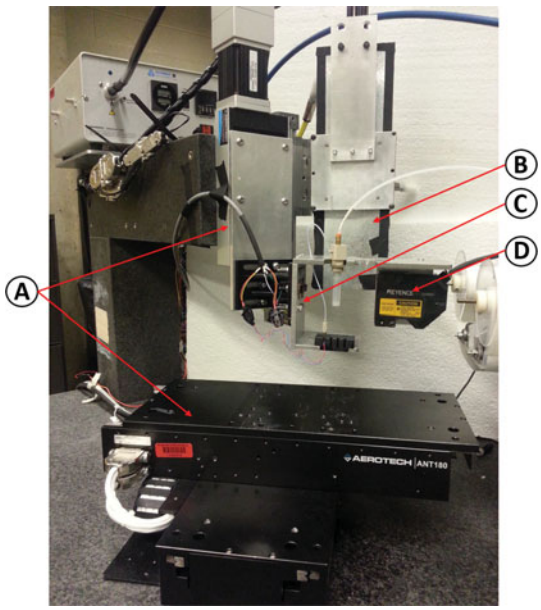

Fig. 16. Experiment setup. (A) Three-axis linear stage, (B) UV curing system, (C) ink-jet bracket, (D) height profile measurement system.

material and object part, in which the sacrificial material should be washed away/removed and the object part is then obtained.

B. Experimental Setup

Fig. 16 shows the overview of the ink-jet 3-D printing system. It consists of a Microfab ink-jet nozzle array, a three-axis Aerotech linear stage, a UV curing system, and a Keyence surface profile measurement system. The substrate is placed on the three-axis linear stage and customized by printing a layer of ink onto silicon wafer to ensure the interaction between layers is always the same. The nozzle is placed above the substrate and is attached to *Z*-axis of the linear stage. The liquid material cartridge is fed into the nozzle, and connected to an air vacuum pump, which provides the back pressure to hold the ink meniscus at the tip of nozzle. During the layer printing process, the stage carries the substrate and traverses the entire printing region, during which the nozzle deposits droplets at the required places on the substrate. After each layer is printed, the stage sends the substrate to a specific location where the UV curing process is carried out to solidify the liquid droplets.

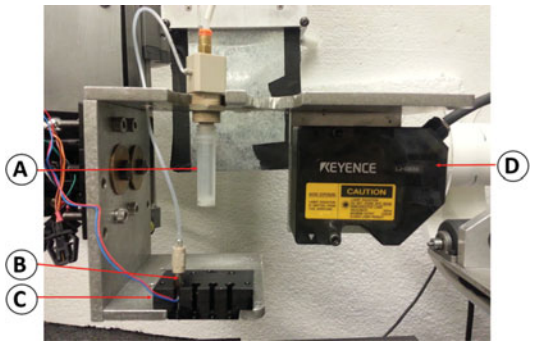

Fig. 17. Ink-jet and measurement system. (A) Ink-jet reservoirs, (B) nozzle, (C) heat block, (D) measurement device.

As shown in Fig. 17, the ink-jet system is composed of a heating block with four nozzle slots, two ink reservoirs, nozzles, and a jet controller. The heating block could be heated up to 45°, which is the working temperature for following experiments. The measurement device is a 2-D laser profile sensor from Keyence. It has 0.1-μm resolution in *Z*-axis, 5-μm resolution in the *X*-axis and varying resolution in *Y*-axis depending on the scanning speed and data storing rate. The repeatability in *Z*-axis height measurement is $1\ \mu$m. The 3-D height profiles can be obtained by scanning across the substrate. The entire laser scanning process for each layer takes about 6 s, and is less than $1/50$ compared to the time duration of the printing process and the UV curing process, which takes more than 5 min for each layer.

The stage is rated to have a nanometer encoder and submicrmeter precision. The droplet deposition signal is generated from stage controller when the stage arrives at preprogrammed positions. In order to solidify the material, an UV lamp is used to cure each layer after deposition.

C. Model Identification

To identify the height change model, three sets of experiments are conducted to find out how droplet deposition layout will affect the height change. The substrate is coated with the ink material to guarantee the consistency between current layer and last layer in terms of material interaction. During each experiment, each droplet immediately cured after deposition to avoid droplets coalescence.

The droplet size is around $410\,\mu$m with a few micrometers variation and the spacing L_x (here, we let $L_x = L_y$) between droplets is $256.988\,\mu$m, which corresponds to 63% of droplet diameter (thus, $\gamma = 0.63$) . The spacing was determined to achieve consistent height for any $n \times n$ matrix droplet layout. The following three steps were then performed to identify the height change constants h_1, h_2, and h_3. It is noted that due to the relatively large repeatability in *Z*-axis height measurement ($1\ \mu$m),

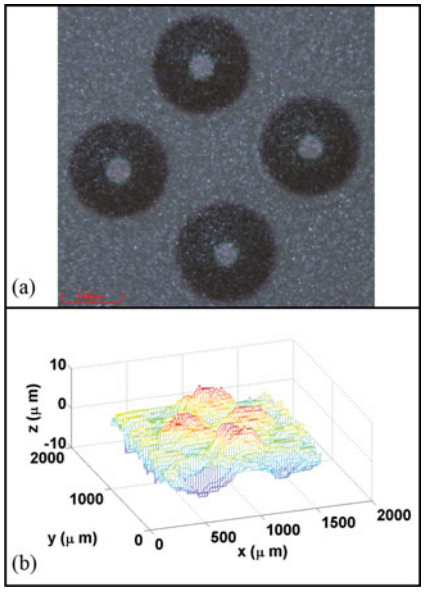

Fig. 18. (a) Top view of four separated droplets: diameter is measured at $413\,\mu\mathrm{m}$; (b) aerial view of four separated droplets: h_1 is the height change factor for the center location due to droplets deposited at center locations which is found to be $4.4\,\mu\mathrm{m}$.

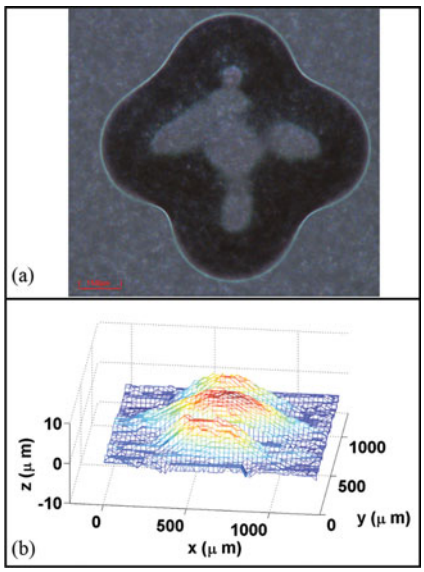

Fig. 19. (a) Top view of side neighbor droplets effect; (b) aerial view of side neighbor droplets effect, h_2 is the height change factor for the center location due to droplets deposited at side neighbors which is found to be $0.6\,\mu\mathrm{m}$.

we conduct a large number of experiments and take the average value for h_1, h_2, and h_3 to minimize the possible errors.

1) *Single Center Droplet:* First, the height and diameter of a single droplet were measured. Fig. 18 shows the top and aerial of four separated droplets. In this case, h_1 is the average peak height of each separate droplet. And the diameter is measured at $413\,\mu\mathrm{m}$ and height change h_1 is found to be $4.4\,\mu\mathrm{m}$.
2) *Side Neighbor Droplets:* Next, an experiment of depositing five droplets is conducted to find out how neighbor droplets will affect the profile height at center location. As seen from Fig. 19(a), there are four side neighbor droplets printed besides the center droplet. The measurements are shown in Fig. 19(b), and the height of center location is increased by $2.4\,\mu\mathrm{m}$, which means that each side neighbor droplet contributes 0.6-$\mu\mathrm{m}$ height addition. Thus, $h_2 = 0.6\,\mu\mathrm{m}$.
3) *Corner Neighbors Droplets:* As shown in Fig. 20, one corner neighbor droplet is deposited to identify how corner neighbor droplet affects the height at center location. The height change parameter h_3 is found to be $0.2\,\mu\mathrm{m}$.

From the three sets of experiments, droplet and model parameters are determined and shown in Table I.

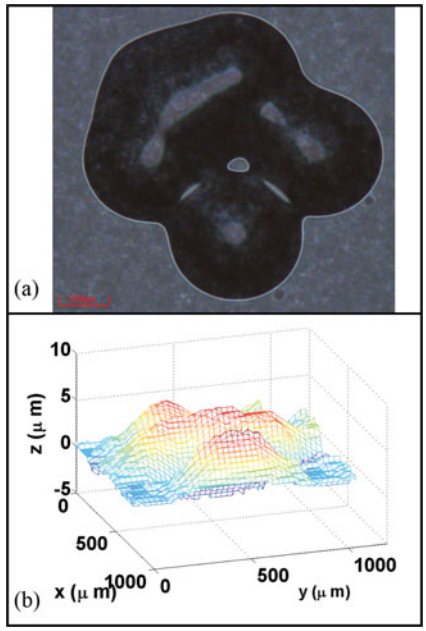

Fig. 20. (a) Top view of corner neighbor droplets effect; (b) aerial view of corner neighbor droplets effect, h_3 is the height change factor for the center location due to droplets deposited at corner neighbors which is found to be $0.2\,\mu\mathrm{m}$.

TABLE I
SYSTEM PARAMETERS

Droplet diameter (d)	$420\,\mu\mathrm{m}$
Droplet spacing ratio (γ)	0.6268
h_1	$4.4\,\mu\mathrm{m}$
h_2	$0.6\,\mu\mathrm{m}$
h_3	$0.2\,\mu\mathrm{m}$

D. Experimental Results

1) Model Verification: To verify the effectiveness of the proposed model. A cuboid was printed to compare with the height profile generated from the model. The cuboid will be four-layer high and printed in open-loop manner, which means that each deposition candidate will be printed. Fig. 22 shows the height profile generated from the proposed model. We can see that it has a shape of a dome. As shown in Fig. 21, the actual

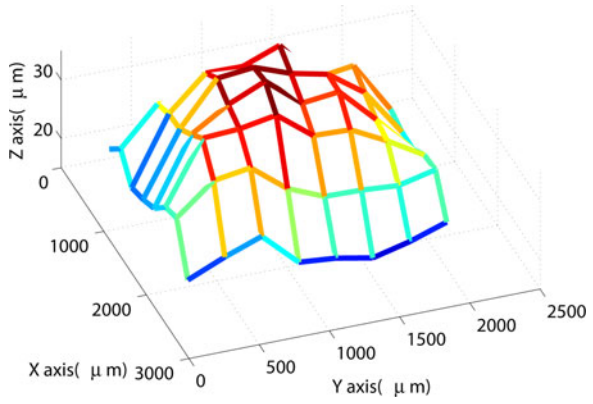

Fig. 21. Measurement of a four-layer open-loop printed cuboid, showing a dome shape.

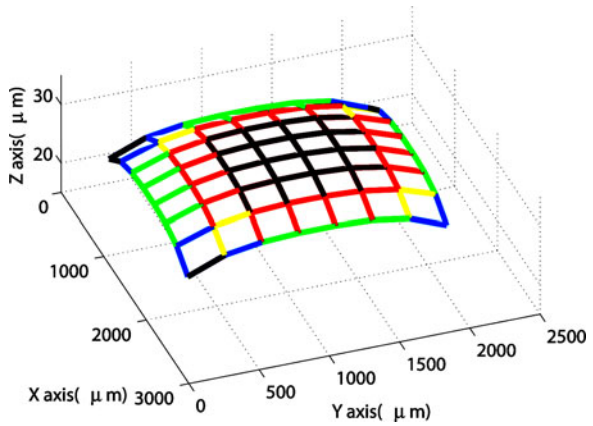

Fig. 22. Proposed model prediction of a four-layer open-loop printed cuboid, also showing a dome shape.

measurement of a four-layer open-loop printed cuboid shows a outline of a dome even with the inclusion of disturbance and uneven substrate. On the other hand, the traditional model simply sums up overlapped region and the predicted profile has constant height over the entire region. Through comparison of the proposed model and traditional model, it is clear that the proposed model is better in modeling the ink-jet 3-D printing process compared with the traditional method.

2) Control Algorithm Verification: Two cuboids were printed to compare the open-loop printing and closed-loop printing performances. The targeted square dimension was $2106.0\,\mu\mathrm{m} \times 2106.0\,\mu\mathrm{m}$ with desired height h_d at $22.8\,\mu\mathrm{m}$. To avoid droplet coalescence, printing patterns in correction procedure were divided into four separated patterns to guarantee that there was no overlapped droplets before curing procedure. The height change parameters are shown in Table I.

The aerial and side views of the two cuboids can been seen in Figs. 23 and 24. For the cuboid printed without any control in Fig. 23, its outline is similar to a dome with large overshoot at center areas and hollow sections at edges. This is due to the nature of the fluid dynamics and small contact angle of the ink. On the other hand, the cuboid printed with correction procedures exhibits much better profile with consistent height

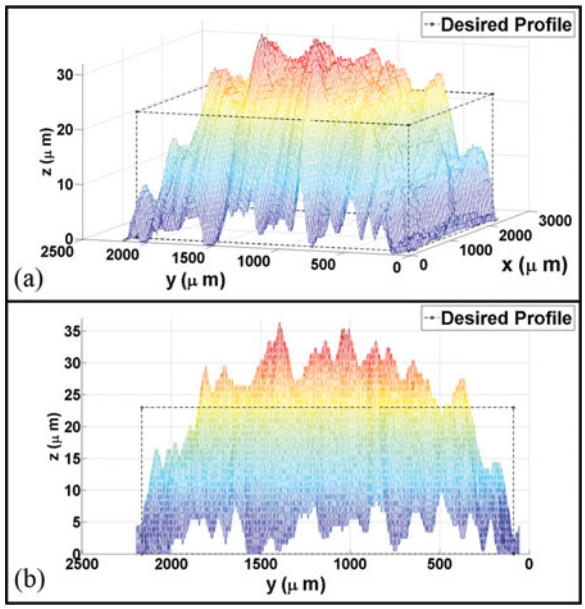

Fig. 23. Open-loop printed cuboid, showing severe edge shrinking and top surface unevenness.

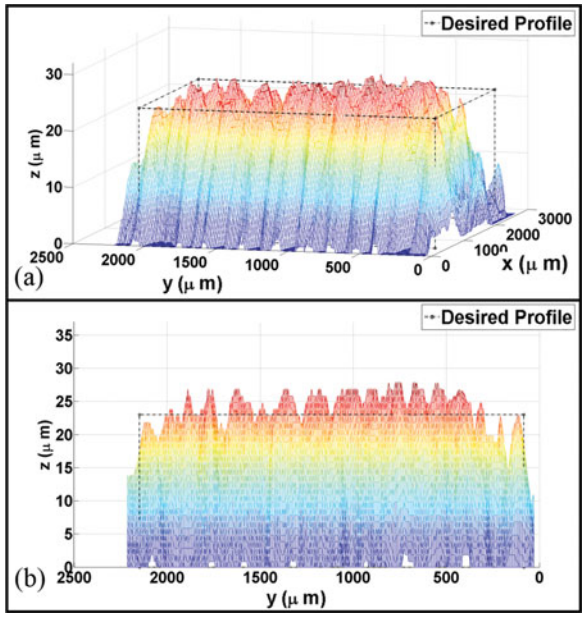

Fig. 24. Closed-loop printed cuboid, showing satisfactory edge profile and surface evenness on the top surface.

in the desired region. Table II shows the comparison between model and two cuboids. It is clear that the cuboid printed with control procedure has very close average height to desired height and its height RMS deviation is about half of the open-loop printed cuboid. However, the *X*- and *Y*-axes measurements of close-loop printed cuboid are about 10% more than the model. This is due to the fact that correction procedures generate many printing tasks on the edges to reach desired height and even top layer. And the droplets on the edges flew over and increased the *X* and *Y* dimension. Although the *X* and *Y*-direction accuracy

TABLE II
EXPERIMENTAL RESULTS

	Ideal Model	Open Loop	Closed Loop
Average Height (μm)	22.8	18.5	22.3
Z-axis RMSD (μm)	0.0	8.7	4.4

are sacrificed for smoother surface and consistent shape, these errors could be corrected later by cutting off the undesired parts.

VI. CONCLUSION

In this paper, a mathematical model was first presented to faithfully reflect the height change caused by droplet deposition during the ink-jet 3-D printing process. A prediction-based layer-to-layer control algorithm based on that model was then proposed to improve the printing quality in terms of the surface evenness and layer height consistency. Experimental results on an ink-jet 3-D printing system showed better performance of the proposed control method compared to the open-loop printing method in terms of achieving desired geometry.

REFERENCES

[1] N. Guo and M. C. Leu, "Additive manufacturing: Technology, applications and research needs," *Frontiers Mech. Eng.*, vol. 8, no. 3, pp. 215–243, 2013.
[2] S. Mishra, K. L. Barton, A. G. Alleyne, P. M. Ferreira, and J. A. Rogers, "High-speed and drop-on-demand printing with a pulsed electrohydrodynamic jet," *J. Micromechanics Microeng.*, vol. 20, no. 9, p. 095026, 2010.
[3] M. L. J. P. Krutha and B. T. Nakagawac, "Progress in additive manufacturing and rapid prototyping," *CIRP Ann. - Manuf. Technol.*, vol. 47, no. 2, pp. 525–540, 1998.
[4] I. Gibson, D. W. Rosen, and B. Stucker, *Additive Manufacturing Technologies*. New York, NY, USA: Springer, 2010.
[5] D. B. W. Patrick W. Cooley and B. V. Antohe, "Applications of ink-jet printing technology to biomems and microfluidic systems," *Adv. Mater.*, vol. 7, no. 5, pp. 33–39, 2002.
[6] B. Derby, "Inkjet printing ceramics: From drops to solid," *J. Eur. Ceramic Soc.*, vol. 31, no. 14, pp. 2543–2550, 2011.
[7] D. L. Cohen and H. Lipson, "Geometric feedback control of discrete-deposition SFF systems," *Rapid Prototyping J.*, vol. 16, no. 5, pp. 377–393, 2010.
[8] Q. Huang, J. Zhang, A. Sabbaghi, and T. Dasgupta, "Optimal offline compensation of shape shrinkage for 3d printing processes," *IIE Trans. Quality Rel.*, to be published.
[9] H. Purwins, B. Barak, A. Nagi, and R. Engel, "Regression methods for virtual metrology of layer thickness in chemical vapor deposition," *IEEE/ASME Trans. Mechatronics*, vol. 19, no. 1, pp. 1–8, Feb. 2014.
[10] C. Doumanidis and E. Skordeli, "Distributed-parameter modeling for geometry control of manufacturing processes with material deposition," *J. Dyn. Syst., Meas. Control*, vol. 122, no. 1, pp. 71–77, 1998.
[11] L. Tang and R. G. Landers, "Layer-to-layer height control for laser metal deposition process," *J. Manuf. Sci. Eng.*, vol. 133, no. 2, 021009 (9 pages), 15 Mar. 2011.
[12] A. Cherala, P. Schumaker, B. Mokaberi, K. Selinidis, B. Choi, M. Meissl, N. N. Khusnatdinov, D. LaBrake, and S. V. Sreenivasan, "Nanoscale magnification and shape control system for precision overlay in jet and flash imprint lithography," *IEEE/ASME Trans. Mechatronics*, vol. 20, no. 1, pp. 122–132, Feb. 2015.
[13] D. B. Soltman, "Understanding inkjet printed pattern generation," Ph.D. dissertation, University of California at Berkeley, Berkeley, CA, USA, 2011.
[14] L. Lu, J. Zheng, and S. Mishra, "A model-based layer-to-layer control algorithm for ink-jet 3d printing," presented at the ASME Dynamic Systems and Control Conf., San Antonio, TX, USA, Oct. 2014.
[15] W. Lee and G. Son, "Numerical study of droplet impact and coalescence in a microline patterning process," *Comput. Fluids*, vol. 42, no. 1, pp. 26–36, 2011.
[16] A. K. Kamrani and E. A. Nasr, *Rapid Prototyping: Theory and Practice*. New York, NY, USA: Springer, 2006.
[17] R. C. Luo, J. H. Tzou, and Y. C. Chang, "Desktop rapid prototyping system with supervisory control and monitoring through internet," *IEEE/ASME Trans. Mechatronics*, vol. 6, no. 4, pp. 399–409, Dec. 2001.
[18] Curse of dimensionality. [Online]. Available: http://en.wikipedia.org/wiki/Curse_of_dimensionality
[19] E. K. P. Chong and S. H. Zak, *An Introduction to Optimization*, 4th ed. New York, NY, USA: Wiley, 2013.
[20] Q. Huang, H. Nouri, K. Xu, Y. Chen, S. Sosina and T. Dasgupta, "Statistical predictive modeling and compensation of geometric deviations of three-dimensional printed products", *J. Manuf. Sci. Eng.* 136(6), 061008 (10 pages), Oct. 24, 2014, Paper# MANU-14-1176; DOI: 10.1115/1.4028510

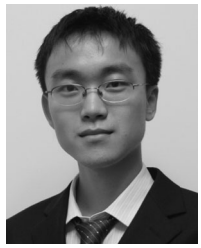

Lu Lu (S'10–M'14) received the M.S. and Ph.D. degrees from the School of Mechanical Engineering, Purdue University, West Lafayette, IN, USA, in December 2010 and August 2013, respectively, and the B.Eng. degree in mechatronic engineering from Zhejiang University, Hangzhou, China, in June 2008.

He has been with the Center for Automation Technologies and Systems, Rensselaer Polytechnic Institute, Troy, NY, USA, since Sep 2013 as Postdoctoral Research Associate. His research interests include control, robotics, manufacturing, sensor fusion and human–machine interaction.

Jian Zheng received the B.S. degree in automation from Shandong University, Jinan, China, in 2012 and the M.S. degree in electrical engineering from Rensselaer Polytechnic Institute, Troy, NY, USA, in 2014.

He is currently working with EcoMotors Allen Park, Michigan, USA, as a Controls Engineer. His main research interests include control, mechatronics, automation, and their applications in additive manufacturing and engine control system.

Sandipan Mishra received the B.Tech. in mechanical engineering from the Indian Institute of Technology, Madras, India, in 2002 and the Ph.D. degree in mechanical engineering from the University of California at Berkeley, CA, USA, in 2008.

He joined the faculty in the Mechanical, Aerospace, and Nuclear Engineering Department, Rensselaer Polytechnic Institute (RPI), Troy, NY, USA, in Fall 2010. He is the Director of the ISAaC Laboratory, RPI, which is supported by grants from NSF, the DoD, and industrial partners including Hewlett Packard Labs, Mathworks, National Instruments and Vivonics Inc. His research interests include the area of systems and control theory, learning control, nonlinear estimation, and precision mechatronics, as applied to smart building systems, additive manufacturing, and adaptive optics.

Dr. Mishra received the NSF Early CAREER Award in 2013 on additive manufacturing and was a member of the 2010 Japan NXT-NSF Young investigator exchange program for nanomanufacturing. He is a Member of the American Society of Mechanical Engineers, and the American Society of Plumbing Engineers.